

Phase-field simulation of superconductor vortex clustering in the vicinity of ferromagnetic domain bifurcations

Hasnain Mehdi Jafri, Jing Wang(王静), Chao Yang(杨超), Jun-Sheng Wang(王俊升), and Hou-Bing Huang(黄厚兵)
Citation: Chin. Phys. B, 2020, 29 (**12**): 127402. DOI: 10.1088/1674-1056/abb22c
Journal homepage: http://cpb.iphy.ac.cn; http://iopscience.iop.org/cpb

What follows is a list of articles you may be interested in

Multiple reversals of vortex ratchet effects in a superconducting strip with inclined dynamic pinning landscape

An He(何安) and Cun Xue(薛存)
Chin. Phys. B, 2020, 29 (**12**): 127401. DOI: 10.1088/1674-1056/abbb

Anisotropy of $Ca_{0.73}La_{0.27}(Fe_{0.96}Co_{0.04})As_2$ studied by torque magnetometry

Ya-Lei Huang(黄亚磊), Run Yang(杨润), Pei-Gang Li(李培刚), Hong Xiao(肖宏)
Chin. Phys. B, 2020, 29 (**9**): 097405. DOI: 10.1088/1674-1056/ab9f26

Topological superconductivity in a $Bi_2Te_3/NbSe_2$ heterostructure: A review

Hao Zheng(郑浩), Jin-Feng Jia(贾金锋)
Chin. Phys. B, 2019, 28 (**6**): 067403. DOI: 10.1088/1674-1056/28/6/067403

Vortex pinning and rectification effect in a nanostructured superconducting film with a square array of antidot triplets

An He(何安), Cun Xue(薛存), Youhe Zhou(周又和)
Chin. Phys. B, 2018, 27 (**5**): 057402. DOI: 10.1088/1674-1056/27/5/057402

Magneto-resistance and vortex phase diagram of $BaNi_{0.1}Fe_{1.9}As_2$ single crystal

Lu Jun-Chao, Yu Yi, Pi Li, Zhang Yu-Heng
Chin. Phys. B, 2014, 23 (**12**): 127402. DOI: 10.1088/1674-1056/23/12/127402

RAPID COMMUNICATION

Phase-field simulation of superconductor vortex clustering in the vicinity of ferromagnetic domain bifurcations*

Hasnain Mehdi Jafri[1,2], Jing Wang(王静)[1,2,†], Chao Yang(杨超)[1,2], Jun-Sheng Wang(王俊升)[1,2], and Hou-Bing Huang(黄厚兵)[1,2]

[1] *School of Materials Science & Engineering, Beijing Institute of Technology, Beijing* 100081, *China*
[2] *Advanced Research Institute of Multidisciplinary Science, Beijing Institute of Technology, Beijing* 100081, *China*

(Received 30 May 2020; revised manuscript received 18 July 2020; accepted manuscript online 25 August 2020)

Superconductors and ferromagnets are highly non-compatible materials due to the natures of their respective electronic states. But when artificially brought together, they develop interesting characteristics, one of which, vortex clustering, is discussed here in this paper. Phase-field and micromagnetic simulations are performed to investigate the superconductor and ferromagnet bilayer, respectively. The ferromagnet with uniaxial anisotropy is observed to develop the maze domain, whereas the superconductor subjected to the influence of the ferromagnetic stray field displays a vortex pattern. Clustered vortices in superconductors at certain locations are observed to be precisely located over magnetic domain bifurcations. The enhanced out-of-plane stray field at bifurcations around the curved domain walls and the convergent Lorentz force due to screening currents in superconductor are attributed to the formation of clusters at bifurcation sites. Segregation of the inter-vortex spacing between straight and bifurcated domain is clearly observed. More importantly, inter-vortex spacing is predicted to serve as a precise tool to map local ferromagnet domain shapes.

Keywords: superconductor–ferromagnet bilayer, vortex pinning, vortex clustering, bifurcated domains

PACS: 74.20.De, 74.25.Wx, 74.25.Uv, 74.78.Fk **DOI:** 10.1088/1674-1056/abb22c

1. Introduction

Most of the superconducting applications are based on the fact that superconductor possesses a high current density, while the presence of dynamic vortices is more likely to be one of the reasons for energy losses.[1] Therefore, during the past decades, much effort has been devoted to better understanding vortex pinning inside type-II superconductors.[2–4] Compared with defects or other types of pinning centers induced by normal metal or insulator inclusions (*e.g.*, Refs. [4–7]), magnetic pinning centers, including nanorod/dot array, templates, domain walls, microloops, *etc.*,[5–9] have proven to be much more promising. More importantly, magnetic pinning of superconducting vortices has led to some very interesting effects including magnetostatic interactions,[10,11] vortex clustering,[12–15] domain wall superconductivity,[16,17] and proximity effects,[1] as well as potential applications of superconducting memories and memristors.[10] In high-κ (where κ is the ratio of London penetration depth and coherence length of superconductor) superconductor–ferromagnet multilayered structures, attractive vortex–antivortex and repulsive vortex–vortex (and antivortex–antivortex) interactions have led the chains and clusters of vortices to form.[13,18,19] Vortex clusters have been observed in non-uniform magnetic field distributions by locally confining magnetic arrangements, controlled by geometric structure of ferromagnet layer, *e.g.*, magnetic dot arrays or voids in ferromagnet layer.[20–22]

In the present study, a magnetostatically coupled superconductor–ferromagnet (SF) bilayer with a thin buffer layer to prohibit electrical contact between both layers, is simulated by micromagnetic simulation using Landau–Lifshitz–Gilbert (LLG) equation for ferromagnets (FM) coupled with the phase-field model using Ginzburg–Landau (GL) equation for superconductors (SC). The FM domain structure is observed to develop in stripe or maze arrangement, with local domain bifurcations. Vortices in the SC layer are observed to be arranged following the FM domain template. Interestingly, vortex clusters are observed at FM domain bifurcations with a wider inter-domain wall spacing, which can be attributed to the locally enhanced out-of-plane stray field and a converged Lorentz force induced by the screening current at bifurcation locations. This research will provide a better understanding of the local pinning of SC vortices in the SF bilayer in particular and maze/stripe-shaped magnetic field arrangements in general, along with a prediction of the vortex clustering and the inter-vortex spacing to be a tool for mapping local magnetic domain pattern. The results presented in this paper can have important implications in the future development of SC vortex-based devices.

*Project supported by the National Natural Science Foundation of China (Grant Nos. 51972028 and 12004036) and the National Key Research and Development Program of China (Grant No. 2019YFA0307900).

†Corresponding author. E-mail: jwang@bit.edu.cn

© 2020 Chinese Physical Society and IOP Publishing Ltd

2. Numerical methods

Coupled LLG equations for FM layer and GL model for SC layer were solved by utilizing in-house developed code. To determine the equilibrium domain structure, the micromagnetic simulations were used, which are based on the dynamic evolution of time-dependent LLG equation[23,24] given below:

$$\frac{\partial \boldsymbol{m}}{\partial t} = -\gamma \boldsymbol{m} \times \boldsymbol{H}_{\text{eff}} - \frac{\alpha_m}{M_s} \boldsymbol{m} \times (m \times \boldsymbol{H}_{\text{eff}}), \tag{1}$$

where $\boldsymbol{m}$ is the normalized magnetization given as $\boldsymbol{m} = \boldsymbol{M}/M_{\text{s}}$, with $\boldsymbol{M} = \boldsymbol{M}(m_x, m_y, m_z)$ being the magnetization vector with the components m_x, m_y, m_z along three coordinate axes; γ, α_m, and M_{s} are the gyromagnetic ratio, damping coefficient, and saturation magnetization, respectively; $\boldsymbol{H}_{\text{eff}}$ is the effective magnetic field.

On the other hand, to study magnetic structure and vortex arrangements in type-II superconductors, a phase-field model was used. Time-dependent GL equations were developed by Gorkov and Eliashberg,[25] and our starting point was the version of equations cited from Refs. [26,27]. Gibbs free energy of SC sample with SC order parameter ψ and magnetic vector potential $\boldsymbol{A}$ is given as

$$G(\psi, \boldsymbol{A}) = \frac{1}{2m} |(\hbar \boldsymbol{\nabla} - \mathrm{i}e\boldsymbol{A})\psi|^2 + \alpha |\psi|^2 + \frac{1}{2}\beta |\psi|^4 + \frac{1}{2\mu_{\text{o}}} |\boldsymbol{\nabla} \times \boldsymbol{A} - \mu_{\text{o}} \boldsymbol{B}|^2, \tag{2}$$

where $\hbar$ is plank's constant, m and e are effective mass and charge of the charge carriers, α and β are phenomenological parameters depending on external factors. A more detailed description of LLG and GL formulism is given in supplementary materials.

3. Results and discussion

The SC and FM layers, separated by a thin insulating buffer layer with a thickness of ξ are simulated for the case of working temperature of 6 K ($T/T_{\text{c}} = 0.645$). The schematic diagram of the bilayer system is shown in Fig. 1. For simplicity, the elemental niobium (Nb) is chosen to be representative of SC family while $CoFe_2O_4$ is chosen to represent FM family for its extensive industrial use in recording and storage media. Both layers are chosen to be 36-nm thick, which corresponds to 3ξ of SC layer, thin enough for the stray field to penetrate uniformly and thick enough to avoid being dominated by any surface effects. A 2000 nm×2000 nm FM layer is simulated with the periodic boundary condition with an 800 nm×800 nm SC island-type structure over it (shape of actual structure is shown as Fig. S1 in Supplementary materials). For simplicity, only that 800 nm×800 nm part of FM layer, which is under SC layer and whose stray field influences the SC layer, is discussed. The calculations are performed by using a home-made code for solving three-dimensional coupled GL and LLG equations for superconductivity and ferromagnetism, respectively. The values of constants used in the present work are listed in the supplementary materials.

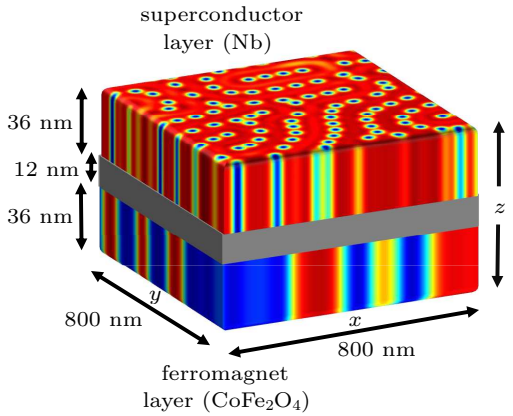


Fig. 1. Schematic diagram of 36-nm-thick SC and FM layers, with 12-nm-thick insulating buffer layer in between to prevent electrical contact in this SF bilayer system.

The FM layer is solved with initial random magnetic distribution with out-of-plane anisotropy, whereas, SC layer was simulated from a completely SC sample (*i.e.*, $|\psi| = 1$) and zero magnetic vector potential ($\boldsymbol{A} = 0$). The SC, under the stray field generated by FM, is relaxed to minimize Gibbs free energy, and then a steady-state vortex pattern is achieved. Under the magnetic stray field generated by the FM domain structure, the vortices (and anti-vortices) (VAV) appear from the boundaries and magnetic domain walls and are rearranged in the domain centers, indicating that the VAV arrangement is strongly dependent on magnetic field patterns.

Figure 2(a) shows the equilibrium FM domain pattern, where red and blue regions indicate positive (perpendicular outward) and negative (perpendicular inward) stripe/maze domain structures in the absence of an external magnetic field, respectively. Figure 2(b) displays the carrier concentration plot of corresponding SC under the stray field generated by FM layer, showing the formation and arrangement of vortices. The vortices can be seen to be aligned with FM domain structure. The SC layer over such a magnetic template develops V-AV pairs above the domain wall and is arranged at the positions of the domain centers due to the position-dependent Lorentz force generated by screening currents in SC layer above the magnetic domains, minimizing the interaction energy between SC and FM layers. Due to a vortex–vortex (and antivortex–antivortex) repulsion (due to non-favoring supercurrent loops) these vortices attain a steady-state with some inter-vortex spacing, depending on the equilibrium of interaction energy (between SC and FM) and free energy of SC layer. Generally, in a flat SC with a uniform magnetic field, vortices are arranged in a hexagonal structure. However, in the case of the magnetic field generated by striped domains, a chainlike distribution of vortices is observed as shown in Fig. 2(b).

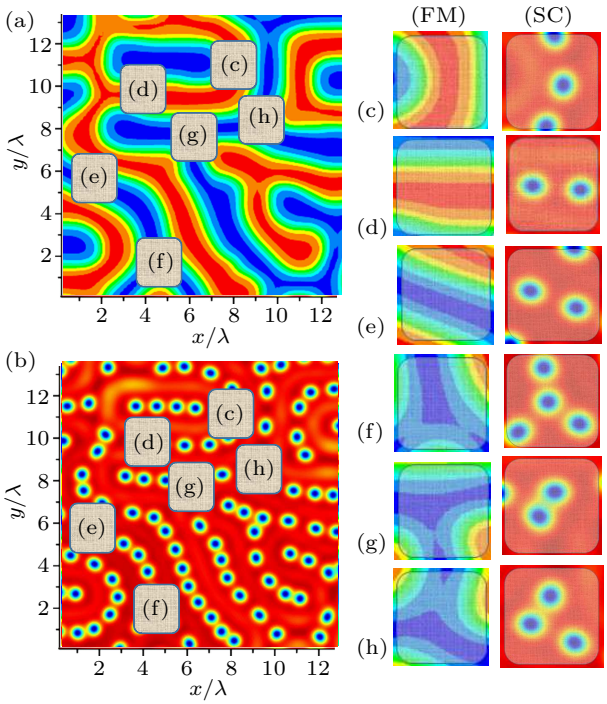


Fig. 2. (a) FM domain pattern with [(c)–(e)] highlighted straight and [(f)–(h)] bifurcated domain regions, with red color representing positive (out of surface) and blue denoting negative (into the plane) domains; (b) corresponding vortex pattern in SC layer with [(c)–(e)] highlighted vortex pattern over straight and [(f)–(h)] vortex pattern over bifurcated FM domains. These highlighted parts are straight FM domain pattern with [(c)–(e)] corresponding (non-clustered) SC vortex pattern and [(f)–(h)] bifurcated FM domains with (clustered) vortex pattern.

The FM domain structure evolved into striped shape with several straight domains is highlighted in the left panels of Figs. 2(c)–2(e), and several bifurcated domains are highlighted in the left panels of Figs. 2(f)–2(h). In the meantime, the corresponding vortex structure is shown alongside the FM domain structure (*i.e.*, the right panel of Figs. 2(c)–2(h)). The vortex clusters are observed in the regions of FM domain bifurcations (Figs. 2(f)–2(h)) compared with the regions above the straight (non-bifurcated) FM domains (Figs. 2(c)–2(e)). These bifurcations provide the enhanced magnetic field in the bifurcation centers compared with the non-bifurcated regions because of larger separation between bifurcation center and neighboring domain center, resulting in the formation of magnetic field pits, which conduces to vortex clustering. These clusters form due to local stray field enhancement, resulting in a reduced inter-vortex repulsion, which can also be attributed to the local variation of Lorentz force caused by screening currents. The local enhancement of the width of bifurcated domains can be seen in Figs. 2(f)–2(h), compared with the width of straight domains in Figs. 2(c)–2(e). The presence of an in-plane component of magnetization at (and in the close vicinity of) domain wall (as there is no out-of-plane magnetization) follows the domain wall curvature in bifurcation region, which is shown by black arrows in Figs. 3(a) and 3(b)) for both straight and bifurcated domains. This flux when reaching the bifurcation region is enhanced due to the in-plane flux from three sides (shown in Fig. 3(b)) and eventually expelled out of the surface in the form of outofplane flux in the bifurcation centers. This field adds to the stray field at the bifurcation region, resulting in the generation of local magnetization pits and thereby enhancing local stray field experienced by SC layer.

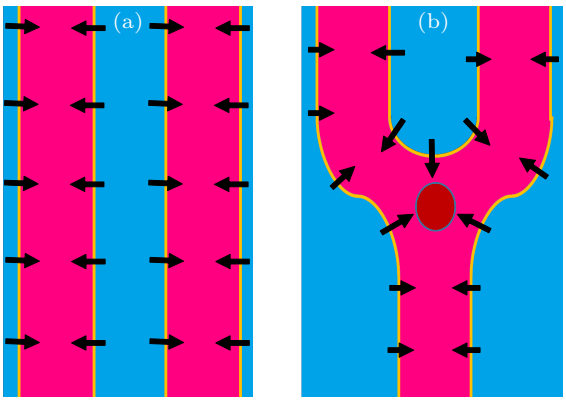


Fig. 3. Sketch showing in-plane magnetizations over the domain walls in FM layer. (a) Straight FM domains and (b) bifurcated striped domains, showing locally enhanced stray field at bifurcation locations resulting in vortex clustering in SC layer.

The vortex structure under the stray field generated by FM clearly shows the formation of vortex clusters corresponding to FM domain bifurcations in Figs. 2(f)–2(h). The Lorentz force at the domain walls, induced by screening currents (as shown in supplementary Fig. S2) and as explained in Fig. 3, drives the vortices away from the domain walls, resulting in a straight-line arrangement of vortices over domain centers, which can be seen in Fig. 2(b). The Lorentz force experienced by each vortex is uniform along the straight domain walls, resulting in vortex arrangements under their inter-vortex repulsive force generated by supercurrent loops around vortices, which, as a result, appear as uniformly spaced vortices, while in the regions of magnetic domain bifurcations, converged Lorentz force results in vortex confinement in the form of clusters. This clustering segregation can be seen in the straight domain wall inter-vortex spacing (IVS) and bifurcated domains IVS in Fig. 4, where carrier concentration is plotted as a function of IVS and the center of the first vortex is taken as the reference point. Curves *a*, *b*, and *c* in Fig. 4 represent straight-walled domains and corresponding vortex arrangement shown in Figs. 2(c)–2(e), respectively; and curves *d*, *e*, and *f* in Fig. 4 denote the domain bifurcations and clustering shown in Figs. 2(f)–2(h), respectively. The IVS is observed to be precisely dependent on the FM domain structure and reduces about 24% in its value from a mean value (taken from a sample of 9 pairs) of 1.11λ for straight domain walls to 0.845λ for cluster region with a variance of 0.12λ. Interestingly, SC penetration depth (λ) can define a barrier between clustered and non-clustered vortices (at $B_z = \kappa/2$) as follows:

$$\mathrm{IVS}|_{B_z=\kappa/2} = \begin{cases} < \lambda, & \text{clustered vortices, bifurcated domains,} \\ > \lambda, & \text{non-clustered vortices, straight domains.} \end{cases} \tag{3}$$

According to the definition from Eq. (3), it becomes very simple to predict the shape of FM domains under the SC by looking at the IVS value in that particular region, and *vice versa*. The complete dataset is included in the supplementary materials.

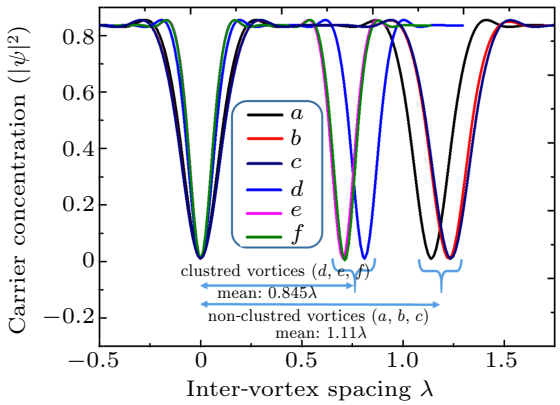


Fig. 4. Segregation of SC vortex clustering with normal vortex spacing under bifurcated and normal FM domain structure. Inter-vortex spacing can be seen to have significant segregation for clustered and non-clustered vortices.

4. Conclusions

A superconductor–ferromagnet bilayer is simulated by using the Ginzburg–Landau equation for superconductors and Landau–Lifshitz–Gilbert equation for ferromagnets, respectively. Vortices are observed to be arranged over the domain centers having uniform spacing over straight domain walls, while they are observed to form clusters, with the inter vortex spacing significantly decreasing (by $\sim 24\%$ in this case) due to locally enhanced stray field and convergent Lorentz force from screening currents. These bifurcations are observed to be random defects in ferromagnets acting as local vortex pinning sites in the superconductor in its vicinity. This clustering affects vortex mobility in superconductors and, in general, enhances the overall efficiency of superconductor–ferromagnet bilayer applications in superconductor–ferromagnet bilayer memories and sensors, and others.

References

[1] Jafri H M, Ma X, Zhao C, Liang D, Huang H, Liu Z and Chen L Q 2017 *J. Phys.: Condens. Matter* **29** 505701
[2] Martin J I, Velez M, Hoffmann A, Schuller I K and Vicent J 1999 *Phys. Rev. Lett* **83** 1022
[3] Jafri H M, Ma X, Zhao C, Huang H, Anwar T, Liu Z and Chen L Q 2018 *J. Supercond. Nov. Magn.* **31** 3445
[4] He A, Xue C and Zhou Y 2018 *Chin. Phys. B* **27** 057402
[5] Kim K, Ozmetin A, Naugle D and Lyuksyutov I 2010 *Appl. Phys. Lett.* **97** 042501
[6] Aladyshkin A Y, Fritzsche J and Moshchalkov V 2009 *Appl. Phys. Lett.* **94** 222503
[7] Vlasko V, Welp U, Karapetrov G, Novosad V, Rosenmann D, Iavarone M, Belkin A and Kwok W K 2008 *Phys. Rev. B* **77** 134518
[8] Silhanek A, Gillijns W, Moshchalkov V, Metlushko V and Ilic B 2006 *Appl. Phys. Let.* **89** 182505
[9] Cao R, Yang T, Horng L and Wu T 2013 *J. Supercond. Nov. Magn.* **26** 2027
[10] Jafri H M, Ma X, Huang H, Zhao C, Qazi H I A, Kazmi S B F, Liu Z, Liu L, Shi S Q and Li Y 2019 *Supercond. Sci. Tech.* **32** 095002
[11] Aladyshkin A Y, Silhanek A, Gillijns W and Moshchalkov V 2009 *Supercond. Sci. Tech.* **22** 053001
[12] DiGiorgio C, Bobba F, Cucolo A, Scarfato A, Moore S, Karapetrov G, D'Agostino D, Novosad V, Yefremenko V and Iavarone M 2016 *Sci. Rep.* **6** 38557
[13] Bespalov A, Mel'Nikov A and Buzdin A I 2015 *Europhys. Lett.* **110** 37003
[14] Nishio T, Dao V H, Chen Q, Chibotaru LF, Kadowaki K and Moshchalkov VV 2010 *Phys. Rev. B* **81** 020506
[15] Grigorieva I, Escoffier W, Misko V, Baelus B, Peeters F, Vinnikov L Y and Dubonos S 2007 *Phys. Rev. Lett.* **99** 147003
[16] Aladyshkin A Y, Buzdin A, Fraerman A, Melńikov A, Ryzhov D and Sokolov A 2003 *Phys. Rev. B* **68** 184508
[17] Buzdin AI and Melńikov A 2003 *Phys. Rev. B* **67** 020503
[18] Bending S J and Dodgson M J 2005 *J. Phys.: Condens. Matter* **17** R955
[19] Samokhvalov A, Savinov D, Mel'nikov A and Buzdin A I 2010 *Phys. Rev. B* **82** 104511
[20] Cieplak M Z, Adamus Z, Kończykowski M, Zhu L, Cheng X and Chien C 2013 *Phys. Rev. B* **87** 014519
[21] Shapoval T, Metlushko V, Wolf M, Neu V, Holzapfel B and Schultz L 2010 *Physica C: Superconductivity* **470** 867
[22] Shapoval T, Metlushko V, Wolf M, Holzapfel B, Neu V and Schultz L 2010 *Phys. Rev. B* **81** 092505
[23] Zhang J and Chen L 2005 *Acta Mater.* **53** 2845
[24] Huang H, Ma X, Liu Z, Zhao C, Shi S and Chen L Q 2013 *Appl. Phys. Lett.* **102** 042405
[25] GoR'Kov L P and Eliashberg G M 1968 *J. Exp. Theor. Phys.* **27** 328
[26] Du Q, Gunzburger M D and Peterson J S 1995 *Phys. Rev. B* **51** 16194
[27] Li M, Gu J, Du L, Zhong H, Zhou L and Chen Q 2020 *Chin. Phys. B* **29** 037401